Sensors & Diagnostics

PAPER

View Article Online
View Journal | View Issue

Cite this: *Sens. Diagn.*, 2023, **2**, 1267

A selective chemosensor *via* click chemistry for Cu^{2+} and Hg^{2+} ions in organic media†

Sachin Kumar, [ab] Bajrang Lal, [a] Ram Kumar Tittal, *[a] Gurleen Singh, [c] Jandeep Singh, [c] Ghule Vikas D., [a] Renu Sharma[b] and Jagjivan K. Sabane[d]

Received 8th May 2023,
Accepted 30th June 2023

DOI: 10.1039/d3sd00109a

rsc.li/sensors

A simple chemosensor, 4-amino antipyrine linked bis-1,2,3-triazole, was synthesized *via* the "click" approach using the CuAAC method and characterized by FTIR, NMR, and ESI-MS spectroscopy. The synthesized chemosensor upon ion sensing study showed a selective and significant detection of Hg(II) and Cu(II) ions, with the LOD being 56 and 63 μM, respectively. Mercury and copper are toxic heavy metals. The quantitative and qualitative detection of these ions is paramount for human health and the environment. The effect of time and temperature on the binding capability of APT with Hg(II) and Cu(II) ions was also studied using UV-Vis spectroscopy. Additionally, DFT studies lay forward the structural optimization of the chemosensor by the (B3LYP)/6-311G(d,p) and B3LYP/LanL2DZ level of theory.

1. Introduction

In recent years, heavy metal exposure has increased due to anthropogenic and agricultural activity and modern industrialization, which negatively impact human health. Worldwide, millions of people are intoxicated by toxic metal contamination in water, air, and food, which are a matter of grave concern for humankind and the complete ecosystem of the environment. Among them, mercury and copper are toxic heavy metals that can cause severe health problems in humans and wildlife. Copper in surface waters occurs predominantly in Cu(II) cupric form. Mercury is a naturally occurring element found in air, water, and soil in various forms: elemental (or metallic) and inorganic (to which people may be exposed through their occupation), and organic (*e.g.*, methylmercury, to which people may be exposed through their diet). Exposure to mercury, even in small amounts, may cause serious health problems. The toxicity and potential of mercury may bio-accumulate and be biomagnified in the food chain, leading to severe health problems such as neurological disorders, renal failure, and congenital disabilities.[1] The permissible limit of Hg and Cu in human physiology according to the World Health Organisation (WHO) and Indian Standard Institutions (ISI) is (0.001 mg l^{-1} and 0.001 mg l^{-1}) and (1.0 mg l^{-1} and 0.05 mg l^{-1}), respectively.[2] Beyond this limit, the aforementioned harmful effects may appear. Therefore, quantitative and qualitative detection of essential trace elements is vital to balance the smooth physiological functioning in biological systems. Developing reliable and sensitive sensors for detecting Hg and Cu ions is crucial.

Various analytical methods have been developed for detecting mercury and copper, including atomic absorption spectroscopy[3] (AAS), inductively coupled plasma mass spectroscopy[4] (ICPMS), and electrochemical sensing.[5] However, these techniques require expensive instrumentation, large sample volume, and trained personnel, and are not always suitable for field applications. Therefore, there is a growing demand to develop a low-cost, portable, and reliable sensing platform for metal ion detection.

One promising approach for developing such a sensing platform is to use 1,2,3-triazole linked with a suitable fluorophore as a sensing molecule[6–8] that allows researchers to develop recognition devices that have distinct advantages like low detection limit, naked eye visual changes, *etc.*, over the other techniques mentioned above. 1,2,3-Triazole is a heterocyclic compound containing a five-membered ring with two carbon atoms and three nitrogen atoms that has been extensively used as a building block in synthetic organic chemistry. The biological importance of 1,4-disubstituted 1,2,3-triazoles includes antimicrobial,[9–11] anticancer,[12] antiviral activities,[13] *etc.* It has also been widely used in developing various analytes due to its unique electronic and structural properties, including its complexation ability with

[a] *Department of Chemistry, National Institute of Technology, Kurukshetra, Haryana 136119, India. E-mail: rktittaliitd@nitkkr.ac.in; Tel: +91 1744 233 542*
[b] *School of Applied Sciences, Om Sterling Global University, Hisar, Haryana 125001, India*
[c] *School of Chemical Engineering and Physical Sciences, Lovely Professional University, Phagwara, Punjab 144411, India*
[d] *Division of Organic Chemistry, CSIR-National Chemical Laboratory, Dr. Homi Bhabha Road, Pune 411008, India*

† Electronic supplementary information (ESI) available. CCDC 2254070. For ESI and crystallographic data in CIF or other electronic format see DOI: https://doi.org/10.1039/d3sd00109a

metal ions like mercury and copper. The synthesis of 1,2,3-triazole-based sensors involves the modification of the 1,2,3-triazole ring to introduce functional groups that can interact with metal ions.[14] The improvement can be achieved through synthetic routes, including "click" chemistry,[9,15–17] azide–alkyne cycloaddition,[18,19] and Sonogashira coupling reactions.[20–22] "Click" chemistry is a powerful tool for synthesizing 1,2,3-triazole-based sensors. In this method, azides and terminal alkynes react in the presence of a copper(I) catalyst to form 1,4-disubstituted-1,2,3-triazoles. The resulting 1,2,3-triazoles can further be functionalized with various reactive functional groups to enhance the sensing ability.

Antipyrine and its derivatives have provoked boundless interest, especially in medicine, due to the wide range of pharmacological activities and therapeutic applications, such as the antibacterial, antifungal, analgesic, antitumor, antipyretic, and anti-inflammatory activity of antipyrine.[23–26] A few intriguing fluorescent sensors based on antipyrine have also been produced.[27–30] Most of the effort has been concentrated on synthesis, structure characterization, and biological evaluation of antipyrine derivatives.[31–35] Due to the abovementioned importance, we were interested in scheming and fabricating antipyrine-based materials with potential technological applications. Herein, we report the design and preparation of an antipyrine-based sensor (**APT**) that bears two triazole rings *via* the CuAAC pathway. Other sensor parts, except for the antipyrine core, serve as metal ion-binding sites. The sensing mechanisms and the analytical performance of the presented sensor for mercury and copper detection were also established *via* UV-vis spectroscopy.

2. Results and discussion

As reported, the symmetrical bis-alkyne **1** having an antipyrine ring was prepared using a propargylation reaction. The organic-azide **2** was obtained from the azidation of the chloroacetyl derivative of antipyrine. The proposed probe **APT** named 2,2′-((((1,5-dimethyl-3-oxo-2-phenyl-2,3-dihydro-1*H*-pyrazol-4-yl) azanediyl) bis(methylene)) bis(1*H*-1,2,3-triazole-4,1-diyl)) bis(*N*-(1,5-dimethyl-3-oxo-2-phenyl-2,3-dihydro-1*H*-pyrazol-4-yl) acetamide) was synthesized *via* the CuAAC "click" reaction of the terminal bis-alkyne with an azide, as shown in Scheme 1. The symmetrical bis-alkyne (**1**), organic azide (**2**), and probe **APT** were characterized successfully (detailed in the ESI† file).

2.1 Spectroscopic analysis

2.1.1 FTIR spectroscopy. The FTIR spectroscopy analysis of the terminal bis-alkyne (**1**), organic azide (**2**), and resulting product, 1,2,3-triazole ring *via* click chemistry, showed a high level of agreement with the expected results. The alkyne (**1**) exhibited characteristic peaks at stretching frequencies of 3269 and 2113 cm^{-1}, corresponding to the ≡C–H and C≡C bonds, respectively. Similarly, the presence of the $–N_3$ group in the organic azide (**2**) was confirmed by a peak at 2096 cm^{-1} in its IR spectra. Upon the fusion of alkyne and azide groups, resulting in the formation of the 1,2,3-triazole ring, the peaks at 3269, 2113, and 2096 cm^{-1} in the spectra of the product **APT** disappeared, indicating the formation of a new compound. Additionally, the emergence of a new peak at 3183 cm^{-1} confirmed the presence of –C=C–H structure in the triazole ring.

2.1.2 NMR and mass spectrometry. Confirmation of the successful synthesis of the symmetrical bis-alkyne (**1**) and its 1,2,3-triazole *i.e.*, **APT** was obtained *via* ^1H and ^{13}C NMR spectra. The ^1H NMR spectrum of compound **1** showed a triplet at δ = 2.23 ppm, attributed to the alkynyl protons (≡C–H) of the bis-alkyne, which was absent in the spectrum of **APT**. However, the alkynyl proton appeared in the aromatic region of the ^1H NMR spectrum of **APT**. Furthermore, the $–CH_2–N–$ protons of the bis-alkyne (**1**) appeared in the vicinity of the aromatic 1,2,3-triazole moiety in **APT**, initially detected by the downfield shift of the peak at δ = 3.96 ppm in the bis-alkyne (**1**). The peaks at δ = 72.26 ppm and δ = 80.74 ppm corresponding to the C≡C bonds in the ^{13}C NMR spectrum of the bis-alkyne (**1**) were absent in the 1,2,3-triazole **APT**, confirming the successful formation of the chemosensor **APT**. The confirmation was further supported by the observed molar mass at m/z = 852.38.

2.2 UV-vis analysis

For UV-vis investigations, after optimization of the solution concentration, the concentration of the **APT** solution was adjusted to 0.03 mM for sensing purposes. The absorption maxima of the probe were measured to be at 283 nm. Solutions of metal ions having 0.5 mM concentration of Ba(II), Zn(II), Cu(II), Hg(II), Ca(II), Mg(II), Cd(II), Pb(II), Ni(II), Co(II), Mn(II) and Cr(III) were prepared in DMSO and then evaluated for sensing experiments using the synthesized probe **APT**. Only the solutions of metal ions Hg(II) and Cu(II) were shown to effectively induce substantial changes in the

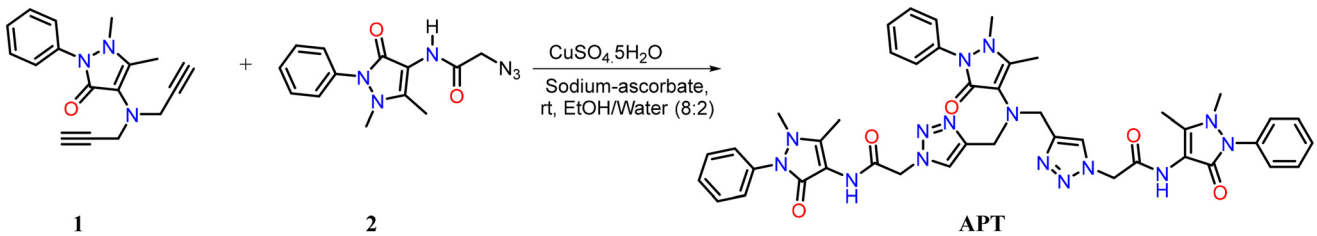

1 2 APT

Scheme 1 Synthesis of the 1,4-disubstituted bis-1,2,3-triazole based probe **APT** *via* CuAAC.

absorption spectra as shown in Fig. 1, while the relative change in the absorption intensity is graphically represented in Fig. 2.

2.3 Chemo-sensing potential of APT

UV-vis spectral analysis was used to investigate the metal ion recognition potential of the probe **APT** with Hg(II) and Cu(II) ions. This was accomplished by titration of 0.03 mM **APT** solution with 15 equiv. of 0.5 mM Hg(II) and Cu(II) solution in discrete instances. The probe concentration was maintained at 0.03 mM throughout the analysis, while the concentration of metal ions was systematically raised from 0 to 15 equiv. On the incremental addition of Hg(II) ions to **APT** solution, the absorption intensity of the latter exhibited a progressive hypochromic shift at 283 nm accompanied by a significant hyperchromic shift leading to the emergence of a sharp peak at 261 nm, with an isosbestic point occurring at 271 nm and hence, verifying the interaction of Hg(II) with the probe **APT**. The absorbance maxima shift (A_n/A_o) *vs.* metal ion molar concentration for the peak at 261 nm with 15 equiv. of Hg(II) ions added in a sequential manner as shown in the inset of Fig. 3, wherein A_n = maximum absorbance, when Hg(II) ions were added incrementally, and A_o = maximum absorbance of the probe. Furthermore, by analyzing the correlation map (Fig. S14†), it was calculated that the LoD (limit of detection) and LoQ (limit of quantification) for Hg(II) is 56 μM and 186 μM, respectively. Also, the stoichiometric ratio between the probe and the metal ion(s) was verified by means of Job plot analysis, wherein different solutions containing **APT** and the metal ion were prepared by holding the total molar concentration constant while altering the molar ratio of **APT** (or metal ion) from 0.1 to 0.9. Fig. S16† shows the relationship between the molar concentration of the metal ions and the relative absorbance change; a threshold at the 0.7 molar ratio suggests a 2 : 1 (M : L) stoichiometry, which are collectively presented in Table 1.

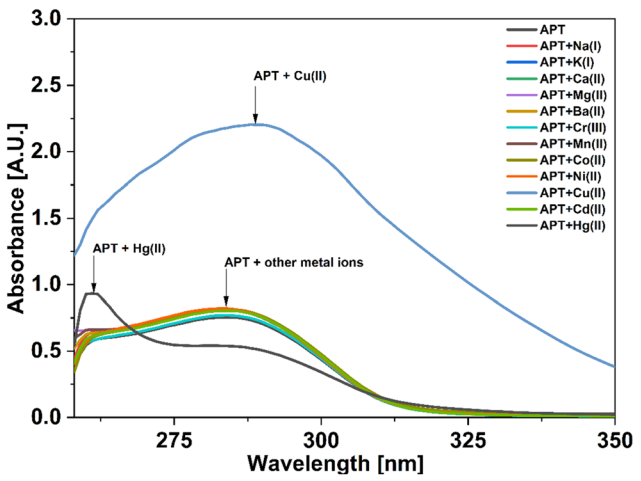

Fig. 1 UV-vis absorption spectra of **APT** with the addition of various metal ions.

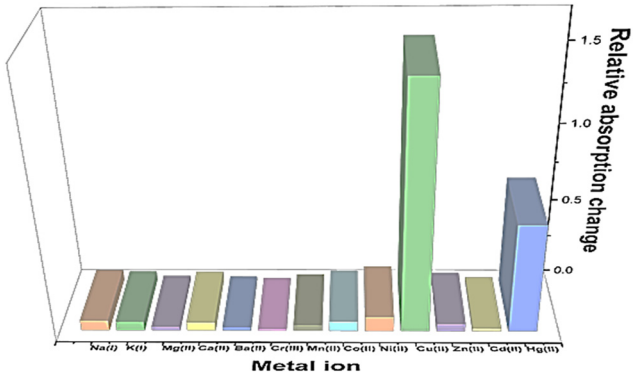

Fig. 2 Relative absorption changes of **APT** with various metal ions in DMSO.

In the case of Cu(II) ions, a progressive addition of Cu(II) ion solution to the 0.03 mM solution of **APT** exhibited a hyperchromic shift at 283 nm, with a slight bathochromic shift of about 3–4 nm, thereby establishing the sensing potential of **APT** for Cu(II) ions also. The absorbance maxima shift (A_n/A_o) *vs.* metal ion molar concentration for the peak at 283 nm with 15 equiv. of Cu(II) ions added in a sequential manner as shown in the inset of Fig. 4, wherein A_n = maximum absorbance, when Cu(II) ions were added incrementally, and A_o = maximum absorbance of the probe. Furthermore, by analyzing the correlation map (Fig. S15†), it was calculated that the LoD and LoQ for Cu(II) are 63 μM and 212 μM, respectively, with a binding ratio of 2 : 1 (M : L), which are also collectively presented in the above mentioned Table 1.

Furthermore, the Benesi–Hildebrand (B–H) equation (I) was used to calculate the association constant (K_a) for the 2 : 1 metal–**APT** complexation with respect to Hg(II) and Cu(II) ions, and the associated B–H graphs are shown in Fig. S17 and S18.† The K_a values for the **APT**–metal complexation were determined

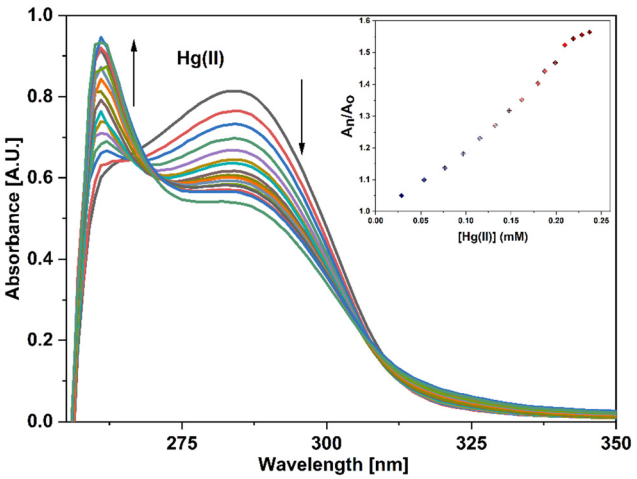

Fig. 3 Progressive changes in the absorption spectrum of **APT** on incremental addition of 15 equiv. of Hg(II) ions; the inset shows the relationship between the relative absorbance of **APT** (A_n/A_o) and the molar concentration of the ion (mM).

Table 1 LoD, LoQ, and stoichiometric binding of **APT** with Cu(II) and Hg(II) ions

Probe	Metal ion	LoD (μM)	LoQ (μM)	Association constant (K_a)	Stoichiometry (M : L)
APT	Hg(II)	56	186	7.34×10^3 M^{-1}	2 : 1
APT	Cu(II)	63	212	4.43×10^4 M^{-1}	2 : 1

to be 7.34×10^3 M^{-1} for Hg(II) and 4.43×10^4 M^{-1} for Cu(II) as presented in the above mentioned Table 1.

2.3.1 Competitive metal ion studies. Competitive ion titration of a 0.03 mM probe solution in DMSO with a solution containing an equimolar concentration of multiple metal ions demonstrated the probe's practical usefulness to preferentially detect Cu(II) independent of the presence of other metal ions. Based on the absorption spectrum (Fig. 5) obtained after the titrations, it seemed that the sensor probe's capacity to identify Cu(II) was unaffected by the presence of other metal ions. However, some significant diminishing in the intensity of absorbance was observed. Additionally, it was also determined from the spectrum that the probe had a binding preference for Cu(II) over other metal ions.

In addition, UV-vis spectroscopy was also employed to examine the probe's propensity for preferentially sensing either Hg(II) or Cu(II) in the presence of both metal ions. The absorption spectrum obtained when the probe solution was titrated with an equimolar solution of Hg(II) and Cu(II) ions was identical to that obtained for Cu(II), as shown in Fig. 4, demonstrating the probe's stronger selectivity for Cu(II) over Hg(II) (Fig. 6).

2.3.2 Time-dependent analysis. After analyzing the influence of time on the binding of **APT** with both metal ions, *i.e.*, Hg(II) and Cu(II), for twenty minutes, the spectral data (Fig. S19 and 20†) revealed that the absorption intensity of the **APT** solution with added Hg(II) as well as Cu(II) ions was not dependent on the time at any point throughout the study. In addition, the aforementioned metal ion solutions, when added to the probe solution, displayed immediate changes in absorption, which indicated that the probe **APT** is an effective "no-wait" sensor for Hg(II) and Cu(II).

2.3.3 Temperature-dependent analysis. The impact of temperature on the probe's binding efficiency was also measured across a wide range of conditions. A positive link between the absorbance of Hg(II)/Cu(II)-bound **APT** and temperature was established as a result of the observation that the absorption spectrum of **APT** displayed a mild rise in the absorption intensity on a steady increase in the temperature from 20 °C to 50 °C. Fig. S21 and S22† represent the spectra of Hg(II)-bound **APT** and Cu(II)-bound **APT** at 2 °C intervals from room temperature up to 50 °C.

3. Computational studies

Density functional theory has become an important tool for computational studies, which acts as a potential instrument for providing structural understanding, especially in organic molecules with extended conjugation, and interpreting several physiochemical properties such as the energy gap ($\Delta E_{LUMO-HOMO}$). The stability and geometrical optimization of the synthesized probe **APT** were also explored using DFT calculations. The geometrically optimized structures of the alkyne (**1**), azide (**2**), and **APT** along with complexes such as **APT.Cu** and **APT.Hg** were obtained by the DFT basis set B3LYP/6-311G(d,p) and B3LYP/LanL2DZ level of theory using the Gaussian 09 package[36,37] as illustrated in Fig. S23–S25.† Additionally, the frontier molecular orbital diagrams with an

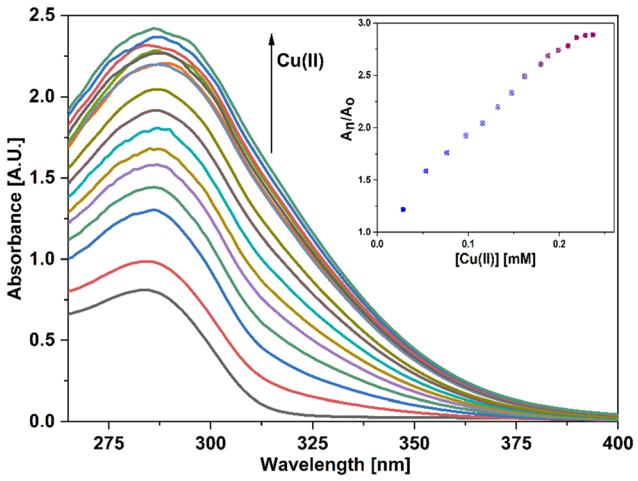

Fig. 4 Progressive changes in the absorption spectrum of APT on incremental addition of 15 equiv. of Cu(II) ions; the inset shows the relationship between the relative absorbance of APT (A_n/A_o) and the molar concentration of the metal ion (mM).

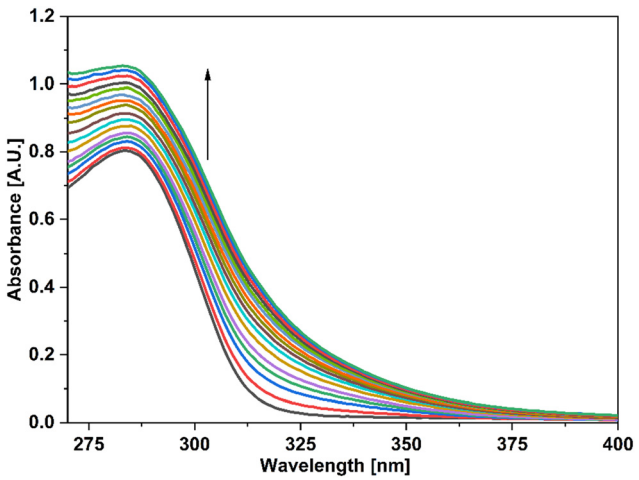

Fig. 5 UV-vis spectra of the probe APT signifying the recognition of Cu(II) among various metal ions present in equimolar concentration.

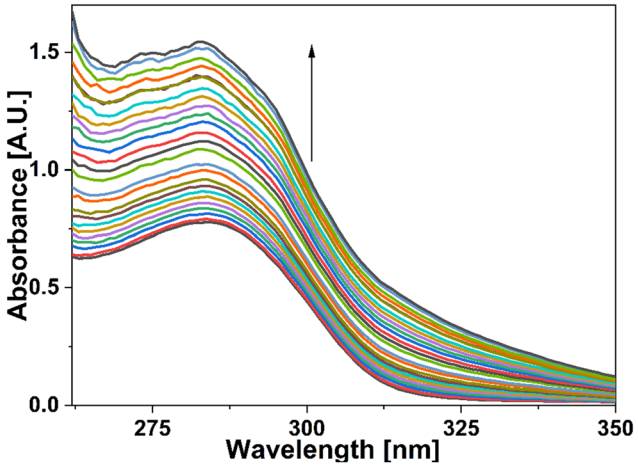

Fig. 6 Absorption spectrum of APT demonstrating the selective recognition of Cu(II) over Hg(II) from an equimolar concentration solution of both metal ions.

energy difference of these optimized molecules (**1**, **2**, **APT**, and **APT.Cu**) are represented in Fig. 7. However, the frontier molecular orbital diagram with an energy difference of the **APT.Hg** optimized molecule is given in Fig. S27.† As clearly depicted in Fig. 7, the band-gap energy of 4-amino antipyrine based 1,2,3-triazole, *i.e.*, **APT** considerably decreases to 4.34 eV as compared to its immediate predecessors, alkyne (4.60 eV) and azide (4.85 eV), which further decreased to 3.55 eV once it formed a complex with Cu, as shown in Table 2. Therefore, the order of the band-gap energy of **1**, **2**, **APT**, and **APT.Cu** is: 2 (4.85 eV) > 1 (4.60 eV) > **APT** (4.34 eV) > **APT.Cu** (3.55 eV). The lowest band-gap energy of the **APT.Cu** complex is due to the probable availability of the metal orbital for accommodating the electron as an acceptor. Surprisingly, the band-gap energy of the **APT.Hg** complex is further decreased to 0.28 eV due to the projection of heavy metal Hg, which can more easily accommodate the electrons to better act as an acceptor.

4. Probable binding mode

The host–guest relationship[38] between triazole of the probe **APT** with Hg(II) and Cu(II) selectively in the presence of other metal ions refers to the specific interaction and recognition between these entities, primarily based on the HSAB principle.[39] According to this principle, which classifies Hg(II) and Cu(II) as weak acids,[40] have a higher affinity for **APT** as the ligand cavity is compatible b/w these two, compared to other metal ions. The 1,2,3-triazole moiety of **APT** can bind to the electron-deficient metal ions *via* different lone pair bearing N and O atoms. Since the Job's plot of **APT** corresponds to a 2 : 1 stoichiometry of metal–ligand, and the 1,2,3-triazole moiety's N atoms and the ligand's O

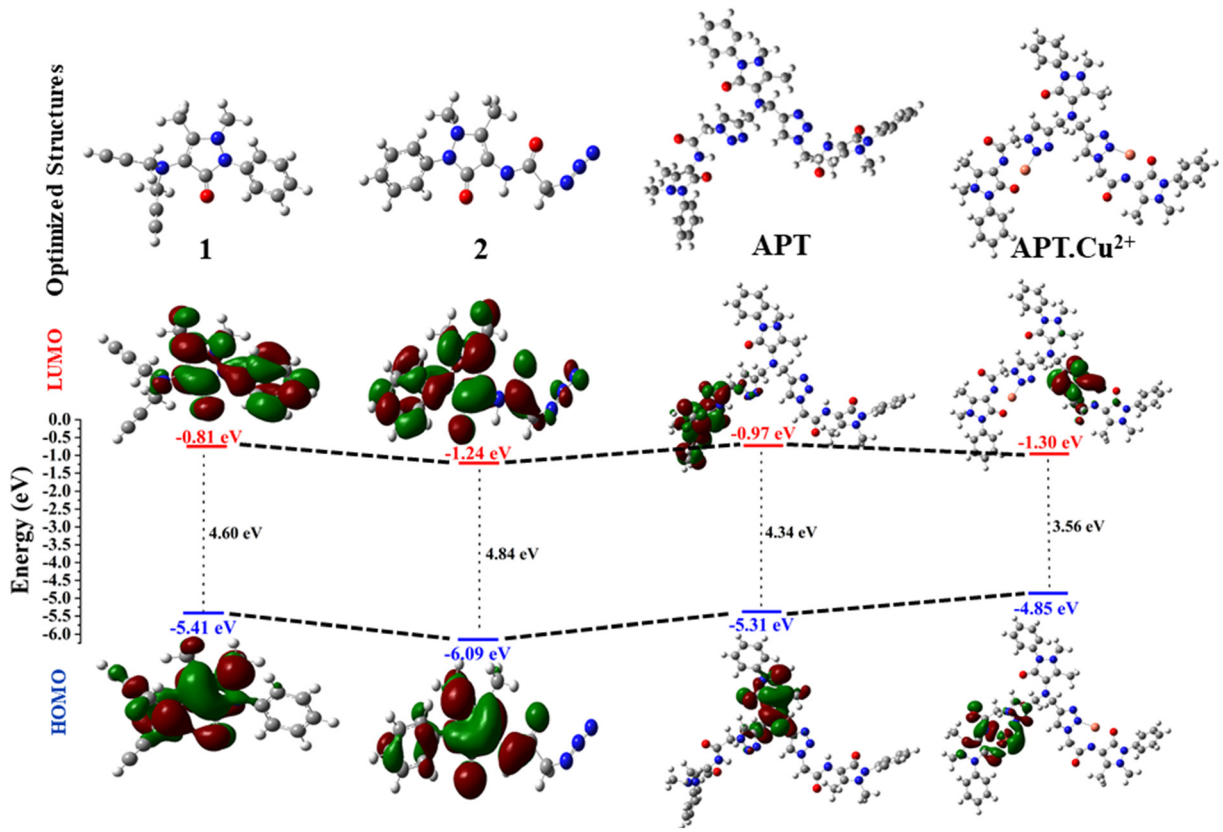

Fig. 7 Optimized structures (**1**, **2**, **APT**, and **APT.Cu**) with the (B3LYP)/6-311G (d,p) and B3LYP/LanL2DZ level of theory *via* the Gaussian 09 package along with their contour plots.

Table 2 Calculated FMOs and energy gap in eV at the B3LYP/6-311G(d,p) and B3LYP/LanL2DZ level of theory

S. no.	Compound	HOMO	LUMO	$\Delta E_{LUMO-HOMO}$
1.	**1**	−5.41	−0.81	4.60
2.	**2**	−6.09	−1.24	4.85
3.	**APT**	−5.31	−0.97	4.34
4.	**APT.Cu**	−4.85	−1.30	3.55
5.	**APT.Hg**	−4.07	−3.79	0.28

atoms can be attributed to being involved in the metal ion binding, the other valency is satisfied by the solvent molecule. Therefore, based on these instances, a proposed mode of interaction between **APT** and metal ions has been portrayed in Fig. 8.

Overall, the host–guest relationship between the probe **APT** and Hg(II) and Cu(II) ions in the presence of other metal ions is based on the hard–soft acid–base principle, which provides a framework for understanding and predicting the preferential binding interactions between metal ions and ligands based on their electronic properties.

5. Experimental

5.1 Materials and methods

All chemicals were purchased from commercially available sources and used without further purification. 4-Amino antipyrine was purchased from (Loba Chemie), propargyl bromide from (Sigma Aldrich), potassium carbonate from (Loba Chemie), chloroacetyl chloride from (Loba Chemie), and sodium azide from (Loba Chemie). Chlorides of various metal ions such as Ba(II), Zn(II), Cu(II), Hg(II), Ca(II), Mg(II), Cd(II), Pb(II), Ni(II), Co(II), Mn(II) and Cr(III) were purchased from Loba Chemie. Solvents were bought from S.D. Fine, Finar, and Loba Chemie. ^{1}H-NMR and ^{13}C-NMR spectra were recorded using a Jeol ECZ 400S instrument with TMS (tetramethylsilane) as a standard internal reference. ESI-MS spectra were recorded using a XEVO G2-XS QTOF spectrometer. FTIR data was obtained from a Shimadzu IRAffinity-1S spectrophotometer. X-ray diffraction data was collected by a Bruker APEX-II CCD diffractometer. A SHIMADZU UV-1900 spectrometer was used for metal ion sensing studies.

5.2 Synthesis and characterization of 4-(di(prop-2-yn-1-yl) amino)-1,5- dimethyl-2-phenyl-1,2-dihydro-3*H*-pyrazol-3-one, 1

Bis-alkyne was prepared by following a known method.[27] For synthesis, 4-amino antipyrine was taken in a round bottom flask and dissolved in 8–10 mL of DMF. K_2CO_3 (2.5 equiv.) was added, and the reaction mixture was stirred for 30 min. After that, propargyl bromide (2.2 equiv.) was added dropwise with constant stirring, and the reaction was allowed to go continuously for another 18 h at room temperature. The reaction progress was monitored with TLC. After completion of the reaction, the workup was facilitated in ice-cold water to get precipitates. The solid that appeared was filtered and washed with plenty of cold water to remove DMF. Further, residues were recrystallized in acetonitrile to obtain the desired product as a brown solid.

Yield: 95%, color: brown solid, m.p. 123–125 °C. FTIR (ν_{max} cm^{-1}): 3269, 3205, 2995, 2933, 2837, 2113, 1651, 1498, 1288 cm^{-1}; ^{1}H NMR (400 MHz, $CDCl_3$) δ 7.48–7.26 (m, 5H), 3.96 (d, J = 4 Hz, 4H), 3.05 (s, 3H), 2.30 (s, 3H), 2.23 (t, J = 4 Hz, 2H); ^{13}C NMR (101 MHz, $CDCl_3$) δ 163.40 (C), 153.83 (C), 135.14 (C), 129.19 (CH), 126.45 (CH), 123.69 (CH), 118.69 (C), 80.74 (C), 77.16 (CH), 72.26 (CH), 42.84 (CH_2), 36.44 (CH_3), 10.83 (CH_3).

5.3 Synthesis and characterization of 2-azido-*N*-(1,5-dimethyl-3-oxo-2-phenyl-2,3-dihydro-1*H*-pyrazol-4-yl)acetamide, 2

First, the chloroacetyl chloride derivative of 4-amino antipyrine was synthesized by following the reported procedure[41] with some modifications. 1 mmol of 4-amino antipyrine was dissolved in 10 mL DCM in a 100 mL round-bottom flask; 1.5 equiv. of K_2CO_3 was added, and the reaction mixture was allowed to stir in an ice bath. A solution of chloroacetyl chloride (1.2 equiv.) was added dropwise to the reaction mixture, and after addition, the ice bath was removed, and the reaction mixture was allowed to reflux for

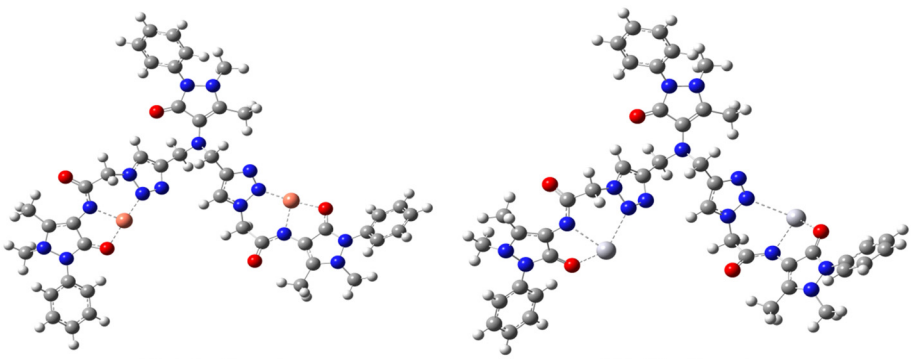

Fig. 8 Proposed binding of the probe **APT** with the electron-deficient metal ions.

10–12 h. On completion of the reaction, as monitored by TLC, the workup was done by filtration followed by evaporation of the filtrate on a rotary evaporator. The solid crude product was washed with plenty of cold water and, after complete drying, used as such for the azidation reaction. The so-obtained solid was dissolved in a minimum amount of acetonitrile. Then, 1.5 equiv. of sodium azide was added to this reaction mixture. On completion of the reaction, the mixture was filtered, and then the filtrate was evaporated on a rotary evaporator. The solid that appeared was washed with cold water and dried under a vacuum to obtain a pale yellow solid.

Yield: 90%, color: pale yellow solid, m.p. 158–160 °C. FTIR (ν_{max} cm^{-1}): 3238, 3207, 3024, 2958, 2096, 1693, 1490, 1307 cm^{-1}. ^1H NMR (400 MHz, $CDCl_3$) δ 9.36 (s, H), 7.32–7.49 (m, 5H), 3.88 (s, 2H), 3.11 (s, 3H), 2.22 (s, 3H); ^{13}C NMR (101 MHz, $CDCl_3$) δ 167.42 (C), 162.13 (C), 150.51 (C), 134.53 (C), 129.86 (CH), 128.07 (CH), 125.35 (CH), 107.72 (C), 52.36 (CH_2), 36.09 (CH_3), 12.61 (CH_3). ESI-MS $[M + H]^+$: m/z cal. for $C_{43}H_{45}N_{15}O_5H^+$ is 287.125, found 287.147. Finally, the solid crystalline material was developed into the single crystal of compound **2** (CCDC no. 2254070), as shown in Fig. 9, upon recrystallization with the solution of ethanol and *n*-hexane. The complete details of the crystal and its structure refinement are given in Table 3. However, the bond length and angles of the obtained single crystal of compound **2** are detailed in Tables 4 and 5, respectively.

5.4 Synthesis and characterization of the probe, APT

The synthesis of the 1,2,3-triazole derivative was performed by following the standard reported procedure. 1 mmol of alkyne **1** was dissolved in 8 mL EtOH in a 50 mL round bottom flask. To this, 2.2 mmol of organic azide **2** was added by dissolving in a minimum amount of EtOH. To the above reaction mixture, copper-sulfate and sodium-ascorbate in 10 and 20 mol%, respectively were added by dissolving each in 1 mL water. The reaction was completed in less than 30 minutes as confirmed by TLC monitoring. After that, the reaction was quenched with ice-cold water to obtain an off-white solid which was washed with 50–100 mL cold water and dried under a vacuum.

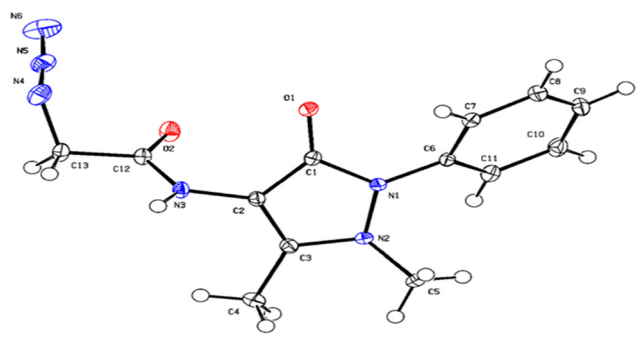

Fig. 9 ORTEP diagram of compound **2** (CCDC no. 2254070).

Yield: 89%, color: off-white solid, m.p. 240–241 °C. FTIR (ν_{max} cm^{-1}): 3265, 3188, 3030, 2922, 2854, 1701, 1309, 759 cm^{-1}. ^1H NMR (400 MHz, $CDCl_3$) δ 9.63 (s, 2H), 7.92 (s, 2H), 7.27–7.50 (m, 15H), 5.28 (s, 4H), 4.27 (s, 4H), 3.04 (s, 6H), 2.80 (s, 3H), 2.11 (s, 6H), 1.75 (s, 3H); ^{13}C NMR (101 MHz, $CDCl_3$) δ 165.06 (C), 161.41 (C), 151.94 (C), 134.88 (C), 129.13 (C), 128.91 (CH), 126.39 (CH), 125.76 (CH), 125.15 (CH), 123.64 (CH), 123.18 (C), 106.57 (C), 51.43 (CH_2), 48.27 (CH_2), 35.90 (CH_3), 11.23 (CH_3), 9.75 (CH_3). ESI-MS $[M + H]^+$: m/z cal. for $C_{43}H_{45}N_{15}O_5H^+$ is 852.3802, found 852.3802.

5.5 Spectrophotometric analysis

The synthesized probe **APT** was analyzed for sensing behavior using UV-visible spectroscopy. Metal ion selectivity was determined with various metal ions such as Ba(II), Zn(II), Cu(II), Hg(II), Ca(II), Mg(II), Cd(II), Pb(II), Ni(II), Co(II), Mn(II) and Cr(III). The sensitivity of the probe **APT** towards Cu(II) and Hg(II) ions was also examined through absorption spectroscopy. Time and temperature-dependent studies, along with competing metal ion titrations were performed for the synthesized probe. The association constant K_a was determined from the B–H plot with the formula K_a = 1/slope, where the slope is determined by plotting 1/conc. of analyte *vs.* 1/change in absorbance. The limit of detection (LoD) was calculated as $3\sigma/k$, and the limit of quantification (LoQ) as $10\sigma/k$, where the standard deviation of the maximum intensity of the probe is denoted by σ. k is the slope of the maximum absorption wavelength intensity as a function of ion concentration.[8]

$$LOD = 3\sigma/k$$

$$LoQ = 10\sigma/k$$

Conclusion

Heavy metals are essential to life in small amounts, but excessive exposure can be toxic. Mercury and copper are two heavy metals that can harm the brain, heart, lungs, kidneys, and immune system when their levels exceed the body's tolerance. Children are particularly vulnerable to mercury exposure as it can impair their neurological development. It's important to be aware of the sources of heavy metals and take steps to minimize exposure. As a result, new affordable methods for detecting such ions are thus required during the time. Considering this, a new chemosensor was synthesized from 4-aminoantipyrine with a "quick-click" approach for the selective detection of Hg(II) and Cu(II) ions with an association constant of 7.34×10^3 M^{-1} and 4.43×10^4 M^{-1}, respectively. This probe exhibited significant changes in its absorption spectra upon the addition of metal ions, allowing for the detection of these metal ions. Additionally, DFT studies were conducted to understand the spatial

Table 3 Crystal data and structure refinement for compound **2**

Compound	**2**
Identification code	mo_SB_0m_a
Molecular structure	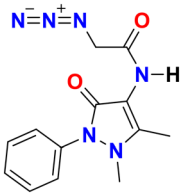
Crystal structure (CCDC: 2254070)	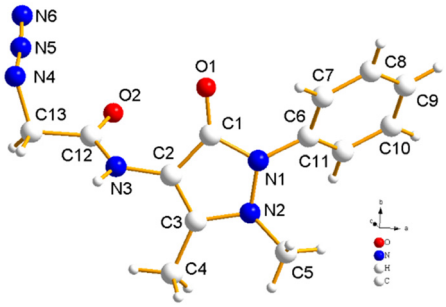
Crystal image	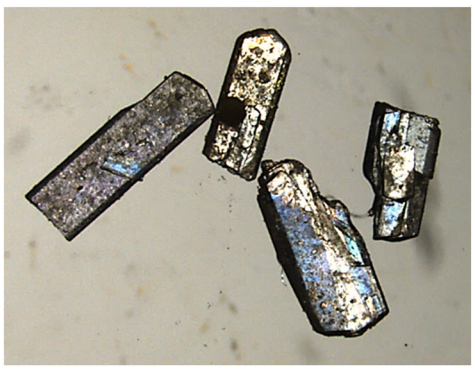
Empirical formula	$C_{13}H_{14}N_6O_2$
Formula weight	286.30
Temperature/K	100(2)
Crystal system	'**Monoclinic**'
Space group	'$P2_1/n$'
a/Å	13.3072(7)
b/Å	6.9369(3)
c/Å	15.2738(9)
α/°	90
β/°	106.507(2)
γ/°	90
Volume/Å^3	1351.82(12)
Z	4
ρ_{calc} g cm^{-3}	1.407
μ/mm^{-1}	0.101
Radiation	MoKα (λ = 0.71073)
2Θ range for data collection/°	4.794 to 68.222
Reflections collected	92 555
Independent reflections	5503 [R_{int} = 0.0871, R_{sigma} = 0.0458]
Data/restraints/parameters	5503/0/192
Final R indexes [$I \geq 2\sigma(I)$]	R_1 = 0.0447, wR_2 = 0.1027
Final R indexes [all data]	R_1 = 0.0751, wR_2 = 0.1143
Largest diff. peak/hole/e Å^{-3}	0.41/−0.32

arrangement of various groups present in the probe through an energy-minimized structure. In order to enhance the capacity of the chemosensor **APT** and derivatives to recognize metal ions in real-world samples, we are currently developing additional testing techniques for upcoming investigations.

Table 4 Bond lengths (Å) of compound 2

Atom 1	Atom 2	Length/Å	Atom 1	Atom 2	Length/Å
O1	C1	1.2404(11)	N5	N6	1.1327(14)
O2	C12	1.2248(11)	C6	C7	1.3937(13)
N3	C2	1.4113(11)	C6	C11	1.3957(13)
N3	C12	1.3510(12)	C2	C1	1.4391(13)
N1	N2	1.4065(11)	C2	C3	1.3576(13)
N1	C6	1.4153(11)	C7	C8	1.3910(13)
N1	C1	1.3851(11)	C11	C10	1.3914(14)
N2	C3	1.3854(11)	C12	C13	1.5211(13)
N2	C5	1.4730(12)	C3	C4	1.4883(13)
N4	N5	1.2349(13)	C8	C9	1.3906(15)
N4	C13	1.4721(14)	C10	C9	1.3886(15)

Table 5 Bond angles (°) of compound 2

Atom 1	Atom 2	Atom 3	Angle/°	Atom 1	Atom 2	Atom 3	Angle/°
C12	N3	C2	120.88(8)	C8	C7	C6	119.33(9)
N2	N1	C6	121.10(7)	O1	C1	N1	124.01(8)
C1	N1	N2	110.55(7)	O1	C1	C2	131.40(8)
C1	N1	C6	126.34(8)	N1	C1	C2	104.55(8)
N1	N2	C5	115.33(7)	C10	C11	C6	119.75(9)
C3	N2	N1	106.01(7)	O2	C12	N3	124.18(8)
C3	N2	C5	120.45(8)	O2	C12	C13	121.03(8)
N5	N4	C13	117.18(8)	N3	C12	C13	114.79(8)
N6	N5	N4	169.59(11)	N2	C3	C4	121.63(8)
C7	C6	N1	118.96(8)	C2	C3	N2	109.69(8)
C7	C6	C11	120.42(8)	C2	C3	C4	128.68(8)
C11	C6	N1	120.61(8)	C9	C8	C7	120.36(9)
N3	C2	C1	124.36(8)	C9	C10	C11	119.91(9)
C3	C2	N3	126.64(8)	N4	C13	C12	110.70(8)
C3	C2	C1	109.00(8)	C10	C9	C8	120.19(9)

Author contributions

Sachin Kumar: methodology, investigation, validation, writing manuscript. Bajrang Lal: methodology, validation. Ram Kumar Tittal: conceptualization, methodology, resources, supervision, writing: review and editing. Gurleen Singh: investigation, validation. Jandeep Singh: conceptualization, resources, writing: review and editing. Vikas D. Ghule: investigation, validation. Renu Sharma: supervision. Jagjivan K. Sabane: investigation, validation.

Conflicts of interest

The authors declare no conflicts of interest.

Acknowledgements

One of the authors, BL acknowledge CSIR-JRF (No.09/1050(0014)/2019-EMR-I) for fellowship and financial assistance. The authors express their gratitude to the National Institute of Technology, Kurukshetra and Lovely Professional University for providing the support and resources that allowed them to complete the present research work.

References

1 M. Balali-Mood, K. Naseri, Z. Tahergorabi, M. R. Khazdair and M. Sadeghi, *Front. Pharmacol.*, 2021, **12**, 1–19.
2 M. Kumar and A. Puri, *Indian J. Occup. Environ. Med.*, 2012, **16**, 40–44.
3 J. W. Robinson, *Anal. Chem.*, 1960, **32**, 17A–29A.
4 S. C. Wilschefski and M. R. Baxter, *Clin. Biochem. Rev.*, 2019, **40**, 115–133.
5 J. Baranwal, B. Barse, G. Gatto, G. Broncova and A. Kumar, *Chemosensors*, 2022, **10**, 363.
6 M. Loya, N. Pramanik, P. Pahari and A. K. Atta, *J. Photochem. Photobiol., A*, 2022, **433**, 114173.
7 A. K. Atta, S. I. Hazarika, M. Loya and S. Giri, *J. Photochem. Photobiol., A*, 2022, **425**, 113723.
8 S. Kumar, S. Gadiyaram, R. K. Tittal, V. D. Ghule and R. Sharma, *J. Mol. Struct.*, 2023, **1290**, 135940.
9 N. Nehra, R. K. Tittal, D. Ghule Vikas, Naveen and K. Lal, *J. Mol. Struct.*, 2021, **1245**, 131013.
10 Naveen, R. K. Tittal, V. D. Ghule, P. Yadav, K. Lal and A. Kumar, *Steroids*, 2020, **161**, 108675.
11 N. Nehra, R. K. Tittal and V. D. Ghule, *ACS Omega*, 2021, **6**, 27089–27100.
12 P. Yadav, K. Lal, A. Kumar, S. K. Guru, S. Jaglan and S. Bhushan, *Eur. J. Med. Chem.*, 2017, **126**, 944–953.
13 Y.-W. He, C.-Z. Dong, J.-Y. Zhao, L.-L. Ma, Y.-H. Li and H. A. Aisa, *Eur. J. Med. Chem.*, 2014, **76**, 245–255.
14 P. Kaur, B. Lal, N. Kaur, G. Singh, A. Singh, G. Kaur and J. Singh, *J. Photochem. Photobiol., A*, 2019, **382**, 111847.
15 G. Singh, R. Singh, N. George, G. Singh, P. Satija, G. Kaur, H. Singh and J. Singh, *J. Mol. Struct.*, 2023, **1277**, 134823.
16 K. Sharma, R. K. Tittal, K. Lal, R. S. Mathpati and V. D. Ghule, *New J. Chem.*, 2023, **47**, 9077.
17 P. Saini, Sushma, G. Singh, G. Kaur, J. Singh and H. Singh, *Inorg. Chem. Commun.*, 2022, **141**, 109524.
18 J. Sultana and D. Sarma, *Catal. Rev.: Sci. Eng.*, 2020, **62**, 96–117.
19 J. R. Johansson, T. Beke-Somfai, A. Said Stålsmeden and N. Kann, *Chem. Rev.*, 2016, **116**, 14726–14768.
20 B. Godlewski, D. Baran, M. de Robichon, A. Ferry, S. Ostrowski and M. Malinowski, *Org. Chem. Front.*, 2022, **9**, 2396–2404.
21 E. M. da Silva, D. Y. de Albuquerque, J. Zukerman-Schpector and R. S. Schwab, *Asian J. Org. Chem.*, 2021, **10**, 1153–1160.
22 I. Kanwal, A. Mujahid, N. Rasool, K. Rizwan, A. Malik, G. Ahmad, S. A. A. Shah, U. Rashid and N. M. Nasir, *Catalysts*, 2020, **10**, 443.
23 M. Hartleb, *Biopharm. Drug Dispos.*, 1991, **12**, 559–570.
24 M. Adithya Krishnan, S. Saranyaparvathi, C. Raksha, B. Vrinda, C. G. Girish, N. V. Kulkarni and B. I. Kharisov, *Russ. J. Coord. Chem.*, 2022, **48**, 696–724.
25 R. Çakmak, E. Başaran, M. Boğa, Ö. Erdoğan, E. Çınar and Ö. Çevik, *Russ. J. Bioorg. Chem.*, 2022, **48**, 334–344.
26 C. J. Dhanaraj and S. S. Salin Raj, *Inorg. Chem. Commun.*, 2020, **119**, 108087.

27 G. Singh, Suman, Diksha, Pawan, Mohit, Sushma, Priyanka, A. Saini and P. Satija, *J. Mol. Struct.*, 2022, **1250**, 131766.
28 G. T. Selvan, M. Kumaresan, R. Sivaraj, I. V. M. V. Enoch and P. M. Selvakumar, *Sens. Actuators, B*, 2016, **229**, 181–189.
29 V. K. Gupta, A. K. Singh and N. Mergu, *Electrochim. Acta*, 2014, **117**, 405–412.
30 J. Dessingou, K. Tabbasum, A. Mitra, V. K. Hinge and C. P. Rao, *J. Org. Chem.*, 2012, **77**, 1406–1413.
31 D. Premnath, P. Mosae Selvakumar, P. Ravichandiran, G. Tamil Selvan, M. Indiraleka and J. Jannet Vennila, *Spectrochim. Acta, Part A*, 2016, **153**, 118–123.
32 P. M. Selvakumar, E. Suresh and P. S. Subramanian, *Polyhedron*, 2007, **26**, 749–756.
33 N. Uramaru, H. Shigematsu, A. Toda, R. Eyanagi, S. Kitamura and S. Ohta, *J. Med. Chem.*, 2010, **53**, 8727–8733.
34 R. Teran, R. Guevara, J. Mora, L. Dobronski, O. Barreiro-Costa, T. Beske, J. Pérez-Barrera, R. Araya-Maturana, P. Rojas-Silva, A. Poveda and J. Heredia-Moya, *Molecules*, 2019, **24**, 1–21.
35 H. M. Y. Al-Labban, H. Mohammed Sadiq and A. A. J. Aljanaby, *J. Phys.: Conf. Ser.*, 2019, **1294**, 052007.
36 M. J. Frisch, G. Trucks, H. B. Schlegel, G. E. Scuseria, M. A. Robb, J. R. Cheeseman, G. Scalmani, V. Barone, B. Mennucci, G. A. Petersson, H. Nakatsuji, M. Caricato, X. Li, H. P. Hratchian, A. F. Izmaylov, J. Bloino, G. Zheng, J. L. Sonnenberg, M. Hada, M. Ehara and K. Toyota, *Gaussian 09, Revision A.02*, Gaussian, Inc., Wallingford, CT, 2009, 227–238.
37 G. Singh, R. Singh, N. George, G. Singh, Sushma, G. Kaur, G. Kaur, H. Singh and J. Singh, *J. Photochem. Photobiol., A*, 2023, **441**, 114741.
38 F. Ahmed and H. Xiong, *Dyes Pigm.*, 2021, **185**, 108905.
39 R. G. Pearson, *J. Am. Chem. Soc.*, 1963, **85**, 3533–3539.
40 R. G. Pearson, *J. Am. Chem. Soc.*, 1963, **85**, 3533–3539.
41 S. Murtaza, A. A. Altaf, M. Hamayun, K. Iftikhar, M. N. Tahir, J. Tariq and K. Faiz, *Eur. J. Chem.*, 2019, **10**, 358–366.